Bulletin of the Seismological Society of America, Vol. 84, No. 6, pp. 1940–1959, December 1994

The Gutenberg–Richter or Characteristic Earthquake Distribution, Which Is It?

by Steven G. Wesnousky

Abstract Paleoearthquake and fault slip-rate data are combined with the CIT-USGS catalog for the period 1944 to 1992 to examine the shape of the magnitude-frequency distribution along the major strike-slip faults of southern California. The resulting distributions for the Newport–Inglewood, Elsinore, Garlock, and San Andreas faults are in accord with the characteristic earthquake model of fault behavior. The distribution observed along the San Jacinto fault satisfies the Gutenberg–Richter relationship. If attention is limited to segments of the San Jacinto that are marked by the rupture zones of large historical earthquakes or distinct steps in fault trace, the observed distribution along each segment is consistent with the characteristic earthquake model. The Gutenberg–Richter distribution observed for the entirety of the San Jacinto may reflect the sum of seismicity along a number of distinct fault segments, each of which displays a characteristic earthquake distribution. The limited period of instrumental recording is insufficient to disprove the hypothesis that all faults will display a Gutenberg–Richter distribution when averaged over the course of a complete earthquake cycle. But, given that (1) the last 5 decades of seismicity are the best indicators of the expected level of small to moderate-size earthquakes in the next 50 years, and (2) it is generally about this period of time that is of interest in seismic hazard and engineering analysis, the answer to the question posed in the title of the article, at least when concerned with practical implementation of seismic hazard analysis at sites along these major faults, appears to be the "characteristic earthquake distribution."

Introduction

It is generally agreed that regional catalogs of seismicity are well described by the Gutenberg–Richter relation

$$\log n = a - bM, \qquad (1)$$

where n is the number of events of magnitude M and a and b are constants (Gutenberg and Richter, 1944; Ishimoto and Iida, 1939). However, whether or not the same distribution is a correct description of seismicity along a specific fault or fault zone seems to remain a question (e.g., Kagan, 1993; Scholz, 1990). Discussion generally revolves around two endmember models. In one, which I will refer to as the Gutenberg–Richter model, it is assumed that seismicity along a given fault or fault zone satisfies equation 1. The model, particularly when applied to seismic hazard analysis, generally implies a relatively stationary process, whereby seismic events of all sizes occur continually on a fault during the interval between the occurrences of the maximum (M^{max}) expected events along the fault zone, and that the size distribution of those events satisfies equation 1 (Fig. 1a). At the other extreme, it is argued that the time between maximum-size earthquakes along particular fault zones or fault segments is generally quiescent, except for the occurrence of foreshocks, aftershocks, and generally low-level background activity. The concept is commonly referred to as the characteristic earthquake model (Schwartz and Coppersmith, 1984), which implies that regional distributions of seismicity that satisfy equation 1 are in part a reflection of the size distribution of faults in the region (Wesnousky *et al.*, 1983), and is illustrated in Figure 1b. Understanding which model is correct is important to seismic hazard analysis. The assumption of either of the two models leads to quite disparate estimates of the return time of moderate but still damaging earthquakes in a region. Similarly, the observed shape of the magnitude-frequency distribution should be manifest in any physical model that portends to explain the mechanical behavior of faults.

Determining which model better describes the general character of seismicity of a particular fault zone is hampered because the historical and instrumental records of seismicity are generally too short to define the repeat time of the largest earthquakes, and hence, the shape of the magnitude-frequency distribution cannot be defined confidently at the largest magnitudes. In contrast, paleoearthquake and geologic fault slip-rate data sample much greater periods of time and, in turn, may be used to independently place limits on the return time of the largest earthquakes along a fault zone, either through direct observation or interpretation within simple mechanical models of fault behavior. Indeed, it was from observation of such data that it was originally suggested that extrapolation of historical earthquake statistics underestimated the recurrence rate of the largest earthquakes along particular fault zones (e.g., Wesnousky *et al.*, 1983; Schwartz and Coppersmith, 1984). Since that time, numerous fault slip-rate and paleoearthquake data have been collected along the major strike-slip faults of southern California. Here I combine paleoearthquake and fault slip-rate data with nearly 5 decades of instrumental recording to examine the shape of the magnitude-frequency distribution along the major strike-slip fault zones of southern California.

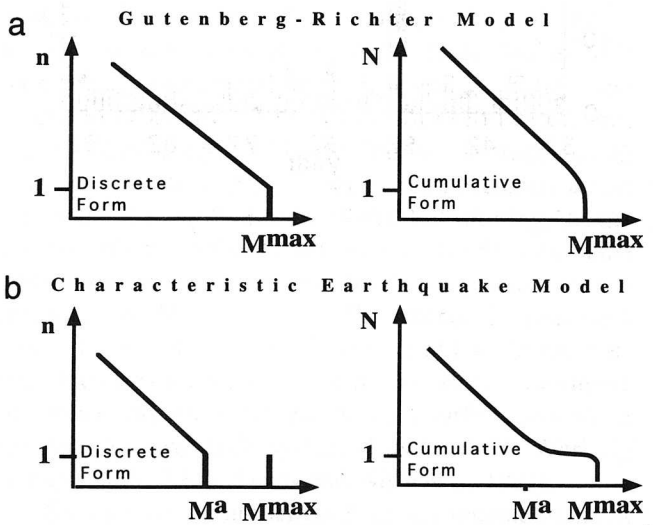

Figure 1. The distribution of the number of events versus magnitude implied by the assumption of either (a) the Gutenberg–Richter or (b) the characteristic earthquake model of fault behavior during the repeat time of one maximum magnitude (M^{max}) event along a fault. Both the discrete and cumulative forms of the expected magnitude distribution, where n equals the number of events equal to a given magnitude and N equals the number of events greater than or equal to a given magnitude, are provided in (a) and (b). For the characteristic earthquake model, the largest earthquake during the repeat time of a maximum-size event is defined to equal the size of the largest aftershock (M^a), and the size distribution of aftershocks is assumed to satisfy the Gutenberg–Richter relationship.

Methodology and Data

The CIT-USGS seismic network has been in operation since 1932. The resulting catalog of seismicity is reportedly complete for events of about $M \geqq 3$ over the southern California region, except for the 1933 Long Beach earthquake sequence (Given *et al.*, 1987). The epicentral distribution of seismicity for the region is shown in Figure 2a. Seismicity recorded within the boxes shown in Figure 2b is the basis to define the rate of occurrence of small to moderate earthquakes along the San Andreas, Garlock, San Jacinto, Elsinore, and Newport–Inglewood faults. Histograms showing the number of events of $M \geqq 3$ versus time for each fault zone are given in Figure 3. Statistical analysis of the earthquake frequency distribution will be limited to the period 1944 to 1992 because, prior to that time, event magnitudes were only reported to the nearest 0.5 magnitude unit. The remain-

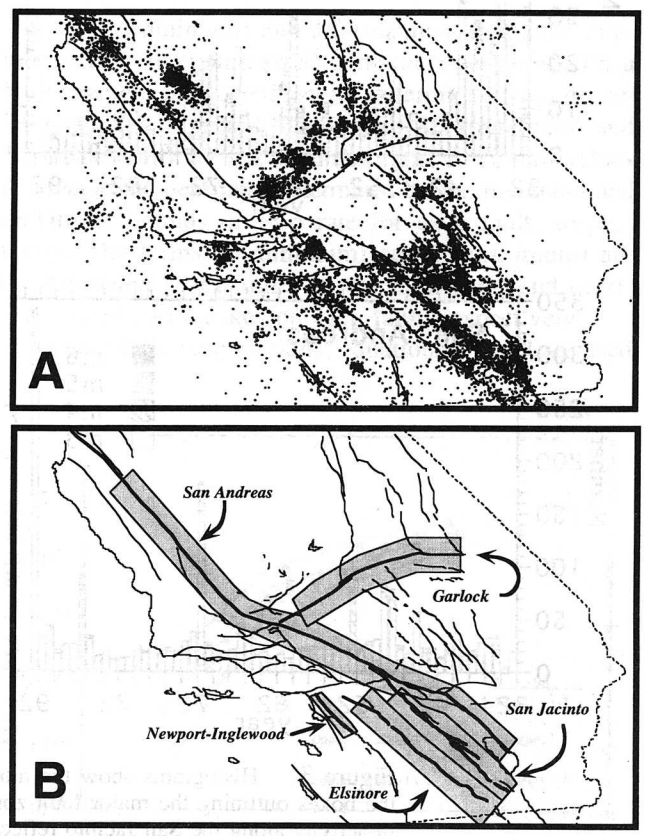

Figure 2. (a) Epicentral map of southern California seismicity ($M > 3$) recorded by the CIT-USGS network for the period from January 1932 through September 1992. (b) The major strike-slip fault zones of southern California considered in this study (bold lines) are encompassed by polygons (shaded).

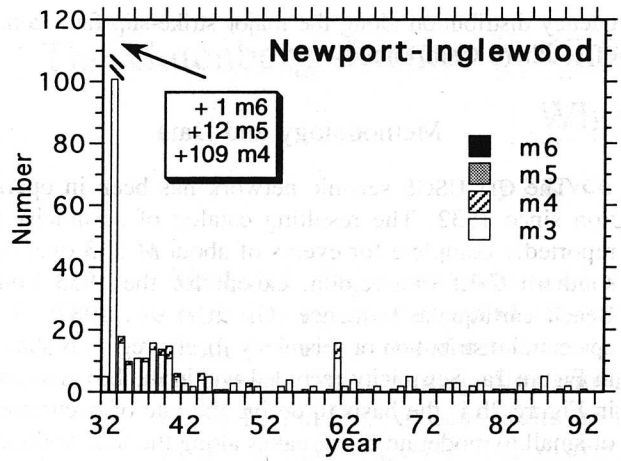

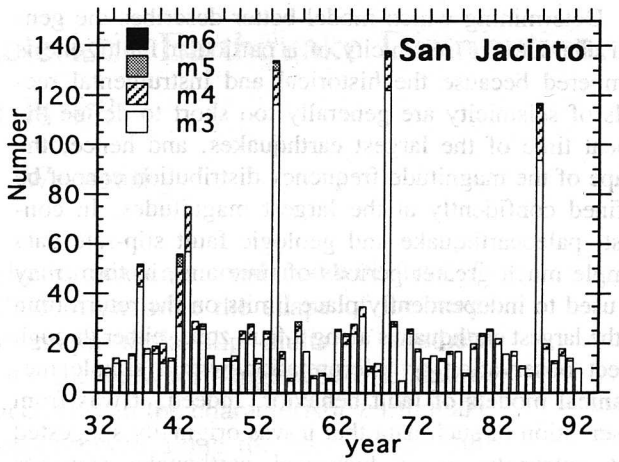

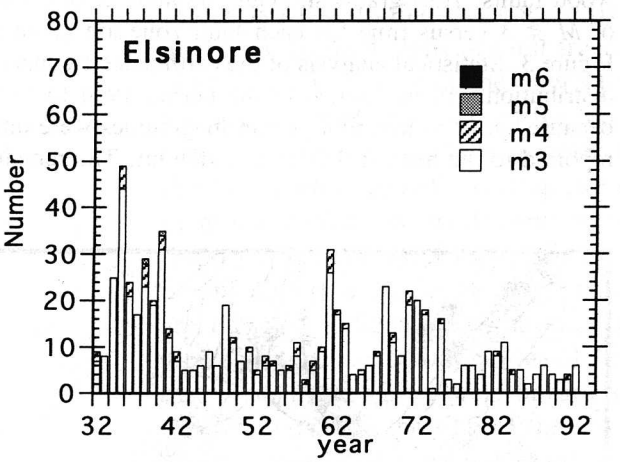

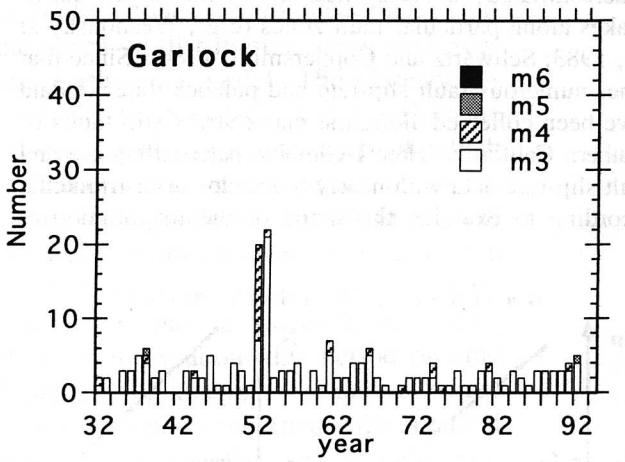

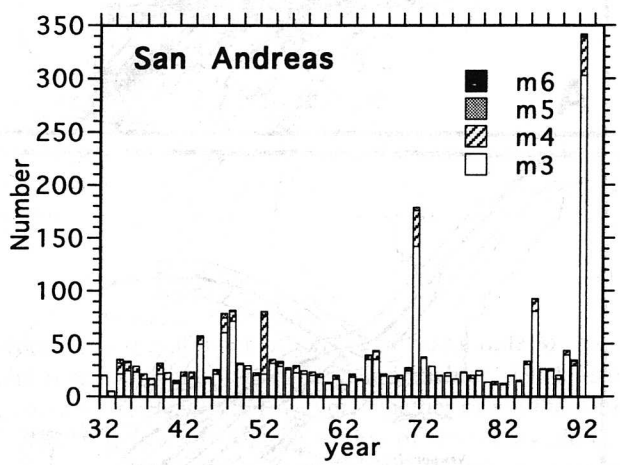

Figure 3. Histograms show the number of events of $M \geqq 3$ per year within the boxes outlining the major fault zones shown in Figure 2b. The large spikes in activity along the San Jacinto reflect the aftershock distributions of the M 6.5 Santa Rosa earthquake of 21 October 1954, the M 6.4 Borrego Mountain earthquake of 9 April 1968, and the M 6.2 and 6.9 earthquakes of November 1987. Similar spikes in activity within other boxes reflect the aftershock distributions of the 1933 M 6.3 Long Beach earthquake along the Newport–Inglewood, the 1971 San Fernando and 1991 Joshua Tree earthquakes on and adjacent to the San Andreas, and the 1952 Kern County earthquake adjacent to the Garlock and San Andreas faults.

der of this section provides a synopsis of the geological observations that place limits on the size and recurrence rate of the largest earthquakes along each of the faults. Combining these latter limits with the seismicity recorded in the CIT-USGS catalog is then the basis to describe the general shape of the magnitude-frequency distribution for each of the major fault zones.

When available, estimates of the average repeat time of the largest expected earthquakes along each of the faults are based directly on the results of paleoearthquake studies or, more specifically, on the interpretation of structural and stratigraphic relations of strata offset by the fault and exposed in trenches. Estimations of the size of the largest expected earthquakes along the faults are based on the amount of offset and the length of rupture registered in past earthquakes. For those sections of fault that have not ruptured historically and where paleoearthquake studies have not provided direct estimates of the repeat time of earthquakes, the recurrence behavior of the largest expected earthquakes along each of the faults is based on the approach outlined in Wesnousky (1986), whereby the average expected repeat time of earthquakes on a fault is approximated to equal $T = (M_0^e/\dot{M}_0^g$ years, where M_0^e is the expected seismic moment for an earthquake on the fault and $\dot{M}_0^g$ is the long-term geologically assessed seismic moment rate of the fault. The seismic moment M_0 is to equal μLWU, where μ is the shear modulus and is taken here to equal 3×10^{11} dyne/cm^2, L is the fault length, W is the fault width (taken as 15 km), and U is the average co-seismic slip occurring across the fault (Aki and Richards, 1980). Substituting $\dot{U}^g$, the geologically determined fault slip rate, for U in the same expression allows us to describe the long-term seismic moment rate $\dot{M}_0^g$ for a fault. The method is consistent with the concept of elastic rebound and has, in essence, been the basis for a number of recent efforts to estimate the probability of occurrence of large earthquakes along the San Andreas fault system (Lindh, 1983; Working Group, 1988, 1990; Sykes and Nishenko, 1984).

Earthquake rupture length L versus seismic moment M_0 is plotted in Figure 4 for the global compilation of historical strike-slip earthquakes reported in Romanowicz (1992). The curves in Figure 4 provide an empirical basis to estimate the expected seismic moment M_0^e of earthquakes on faults or fault segments of length L when direct evidence from the historical or geologic record is not available. The curves are of the form $M_0 = C_0 L^d$, where C_0 and d are empirical constants. The bounding curves in Figure 4 provide minimum and maximum bounds on the expected size M_0^e of an earthquake. The curve labeled "best" provides what I will, for convenience, refer to as the preferred estimate for the expected size of an earthquake to rupture a fault of length L.

Bounds on the seismic moment rate $\dot{M}_0^g$ are a direct function of the maximum and minimum bounds on the fault slip rate $\dot{U}^g$ reported for each fault or fault segment, and the best or preferred estimate of $\dot{M}_0^g$ is based on the preferred estimate of the fault slip rate provided by the reporting investigator. Hence, division of the preferred estimate of M_0^e by the preferred estimate of $\dot{M}_0^g$ yields the preferred estimate of recurrence time T for a given fault or fault segment.

$$T^1 \text{ (preferred)} = M_0^e \text{ (preferred)}/\dot{M}_0^g \text{ (preferred)}. \quad (2)$$

Similarly, extreme bounds on expected recurrence behavior for a given fault segment are found by dividing the minimum and maximum estimates of M_0^e and $\dot{M}_0^g$ in the following manner:

$$T^2 \text{ (minimum)} = M_0^e \text{ (minimum)}/\dot{M}_0^g \text{ (maximum)} \quad (3a)$$

$$T^3 \text{ (maximum)} = M_0^e \text{ (maximum)}/\dot{M}_0^g \text{ (minimum)} \quad (3b)$$

$$T^4 \text{ (minimum)} = M_0^e \text{ (minimum)}/\dot{M}_0^g \text{ (minimum)} \quad (3c)$$

$$T^5 \text{ (maximum)} = M_0^e \text{ (maximum)}/\dot{M}_0^g \text{ (maximum)} \quad (3d)$$

where M_0^e (minimum) and M_0^e (maximum) are the minimum- and maximum-sized earthquakes expected on a fault segment of a given length, determined from the relationships in Figure 4. The values $\dot{M}_0^g$ (minimum) and $\dot{M}_0^g$ (maximum) are the minimum and maximum values of seismic moment rate, determined by the minimum and maximum bounds on slip rate for each fault, respectively. The terms T (minimum) and T (maximum) are the estimated return times of the minimum- and maximum-sized earthquakes on each fault, respectively.

In the following sections, equations 2 and 3 are used

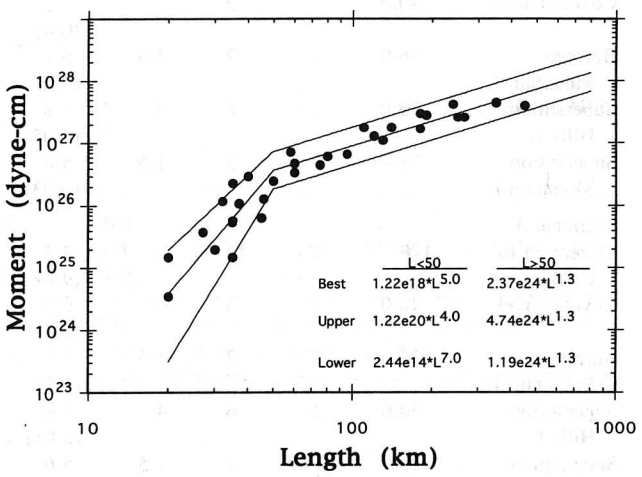

Figure 4. Seismic moment versus rupture length (L) for the global data set of major strike-slip faults listed by Romanowicz (1992). See text for further discussion.

Table 1
Data and Calculations

Fault Segment	Length	Slip Rate (mm/yr) min	Slip Rate (mm/yr) max	Slip Rate (mm/yr) pref	Magnitude* min	Magnitude* max	Magnitude* pref	Repeat Time Estimates† T^1	T^2	T^3	T^4	T^5
San Andreas												
Scenario 1												
Parkfield to Cajon	380	16	43	30	7.5 (26)	7.9 (100)	**7.7** (**54**)	**350**	36	388	98	145
Tejon to Bombay	400	11	35	24	7.6 (29)	8.0 (114)	7.8 (20)	**250**	46	577	145	181
Scenario 2												
Parkfield to Cajon	380	16	43	30	7.5 (26)	7.9 (100)	**7.7** (**54**)	**350**	36	388	98	145
Tejon to Cajon	190	11	35	24	7.2 (11)	7.7 (43)	7.5 (22)	**350**	39	462	116	145
Cajon to Bombay	210	11	35	24	7.3 (13)	7.8 (49)	7.3 (10)	**250**	37	476	119	150
San Jacinto												
Scenario 1												
Claremont	65.0	8	12	9	6.9 (2.7)	7.3 (11)	7.1 (5.4)	204	77	460	115	307
Casa Loma	60	8	12	9	6.8 (2.4)	7.2 (9.7)	7.0 (4.9)	200	75	450	112	300
Clark	50	8	12	9	6.7 (1.9)	7.1 (7.6)	6.9 (3.8)	190	71	425	107	283
Coyote Creek	40.0	1	3	2	6.3 (0.4)	6.9 (3.1)	6.7 (1.2)	374	74	1735	222	578
Borrego Mountain f.	36.0	1	2	1.5	6.1 (0.2)	6.8 (2.0)	**6.5** (**1.0**)	**150**	59	1264	118	632
Superstition Hills f.	30.0	2	6	4	5.8 (0.05)	6.6 (1.0)	**6.6** (**1.0**)	**225**	<10	366	20	122
Superstition Mountain f.	28.0	1	2	1.5	5.6 (0.03)	6.5 (0.7)	6.1 (0.2)	111	13	595	26	297
Scenario 2												
Claremont	65.0	8	12	9	6.9 (2.7)	7.3 (11)	7.1 (5.4)	204	77	460	115	307
Casa Loma to Clark	110	8	12	9	7.1 (5.4)	7.5 (21)	7.3 (11)	239	90	539	135	359
Coyote Creek	40.0	1	3	2	6.3 (0.4)	6.9 (3.1)	6.7 (1.2)	374	74	1735	222	578
Borrego Mountain f.	36.0	1	2	1.5	6.1 (0.2)	6.8 (2.0)	**6.5** (**1.0**)	**150**	59	1264	118	632
Superstition Hills f.	30.0	2	6	4	5.8 (0.05)	6.6 (1.0)	**6.6** (**1.0**)	**225**	<10	366	20	122
Superstition Mountain f.	28.0	1	2	1.5	5.6 (0.03)	6.5 (0.7)	6.1 (0.2)	111	13	595	26	297
Scenario 3												
Claremont to Clark	170	8	12	9	7.3 (9.4)	7.7 (38)	7.5 (19)	273	102	614	154	409
Coyote Creek	40.0	1	3	2	6.3 (0.4)	6.9 (3.1)	6.7 (1.2)	374	74	1735	222	578
Borrego Mountain f.	36.0	1	2	1.5	6.1 (0.2)	6.8 (2.0)	**6.5** (**1.0**)	**150**	59	1264	118	632
Superstition Hills f.	30.0	2	6	4	5.8 (0.05)	6.6 (1.0)	**6.6** (**1.0**)	**225**	<10	366	20	122
Superstition Mountain f.	28.0	1	2	1.5	5.6 (0.03)	6.5 (0.7)	6.1 (0.2)	111	13	595	26	297

Table 1—*Continued*

Fault Segment	Length	Slip Rate (mm/yr) min	Slip Rate (mm/yr) max	Slip Rate (mm/yr) pref	Magnitude* min	Magnitude* max	Magnitude* pref	Repeat Time Estimates† T^1	T^2	T^3	T^4	T^5
Garlock												
Scenario 1												
Entire trace	240	4	9	6	7.4 (15)	7.8 (59)	7.6 (29)	454	152	1363	342	605
Scenario 2												
SAF to Koehn L.	100	4	9	6	7.1 (4.7)	7.5 (19)	7.3 (9.4)	349	117	1048	263	465
Koehn L. to Avawatz	140	4	9	6	7.2 (7.3)	7.6 (29)	7.4 (15)	386	129	1160	291	515
Scenario 3												
Segment 1	60	4	9	6	6.9 (2.4)	7.3 (9.7)	7.1 (4.9)	299	100	899	225	399
Segment 2	80	4	9	6	7.0 (3.5)	7.4 (14)	7.2 (7.1)	326	109	980	246	435
Segment 3	100	4	9	6	7.1 (4.7)	7.5 (19)	7.3 (9.4)	349	117	1048	263	465
Elsinore												
Scenario 1												
Entire trace	240	1.5	9	5	7.4 (15)	7.8 (59)	7.6 (29)	545	147	3635	912	586
Scenario 2												
Whittier	70	1.5	9	5	6.9 (3.3)	7.3 (13)	7.0 (6.5)	384	103	2564	643	413
Corona to L. Elsinore	22	1.5	9	5	5.1 (0.01)	6.2 (0.3)	**6.2** **(0.3)**	**250**	<10	192.5	<10	31
L. Elsinore to Agua Tibia Mtns	50	1.5	9	5	6.8 (1.9)	7.2 (7.7)	7.1 (3.8)	340	91	2271	570	366
Agua Tibia Mtns to Tierra Blanca Mtns	80	1.5	9	5	7.1 (3.6)	7.5 (14)	7.2 (7.1)	392	105	2615	656	421
Tierra Blanca to Coyote Mtns	60	1.5	9	5	7.0 (2.5)	7.4 (9.7)	**6.7** **(1.4)**	**350**	97	2398	602	386
Newport–Inglewood												
Scenario 1												
Onshore trace	62	0.1	6	0.6	6.9 (2.5)	7.3 (10)	7.1 (5.1)	3028	152	36330	9121	605
Scenario 2												
North segment	28	0.1	6	0.6	5.6 (0.03)	6.5 (0.7)	6.2 (0.2)	277	<10	5951	261	99
1933 rupture	34	0.1	6	0.6	6.0 (0.13)	6.7 (1.6)	**6.4** **(0.5)**	603	14	10660	837	177

*Bold and underlined type indicates a value based on the size of a historical earthquake (see text for discussion). Otherwise, values are determined from the relationships in Figure 3. Values of the seismic moment (10^{26} dyne-cm) are also given in parentheses.

†Bold and underlined type indicates a value based on paleoearthquake study (see text for discussion). Otherwise, values are determined from equations 2 and 3.

to characterize the recurrence behavior of faults and fault segments when direct evidence from the geologic and historical record is lacking. Conversion of estimates of M_0^e to moment magnitude M_w with the relationship log $M_0 = 1.5\ M_w + 16.1$ (Hanks and Kanamori, 1979) then allows the recurrence estimates arising from equations 2 and 3 to be combined with the CIT-USGS catalog of seismicity to define the shape of the magnitude-frequency distribution along each fault zone. Table 1 summarizes the bounding estimates of the fault slip rate $\dot{U}^g$, repeat times T^i ($i = 1.5$), expected moment magnitude M_w, and fault lengths for the various rupture scenarios assumed for each of the strike-slip faults that are discussed in the following sections.

The Newport–Inglewood Fault

The fault strikes southeast and offshore of Newport Beach (Fig. 5). The fault produced the magnitude 6.3 ($M_0 \approx 5 \times 10^{25}$ dyne-cm) Long Beach earthquake of 10 March 1933 (Hauksson and Gross, 1991; Richter, 1958). Aftershocks of the 1933 event concentrated along the approximately 30-km segment of the fault extending northwest of the epicenter (Benioff, 1938; Hauksson and Gross, 1991; Richter, 1958). I am not aware of any paleoearthquake studies providing direct estimates of the return time of such earthquakes along the fault, and geological limits on the fault slip rate are poor. Right-lateral slip has reportedly averaged 0.3 to 0.8 mm/yr since the Pliocene (Anderson, 1979; Bird and Rosenstock, 1984). Estimates of slip rate from offset features of the Holocene to the Pleistocene span a large range between 0.1 and 6.0 mm/yr, with preferred values equal to about 0.6 mm/yr (Clark *et al.*, 1984).

Estimates of both M_0^e and $\dot{M}_0^g$ on the right side of equations 2 and 3 require estimates of the expected rupture length of future earthquakes. In that regard, limits on the recurrence behavior for the fault are based on two rupture scenarios. The first reflects the assumption that the entire length of the fault ruptures in repeated earthquakes, and in the second, it is assumed that the fault consists of two independent segments; the 1933 rupture zone and an approximately equal length of fault extend-

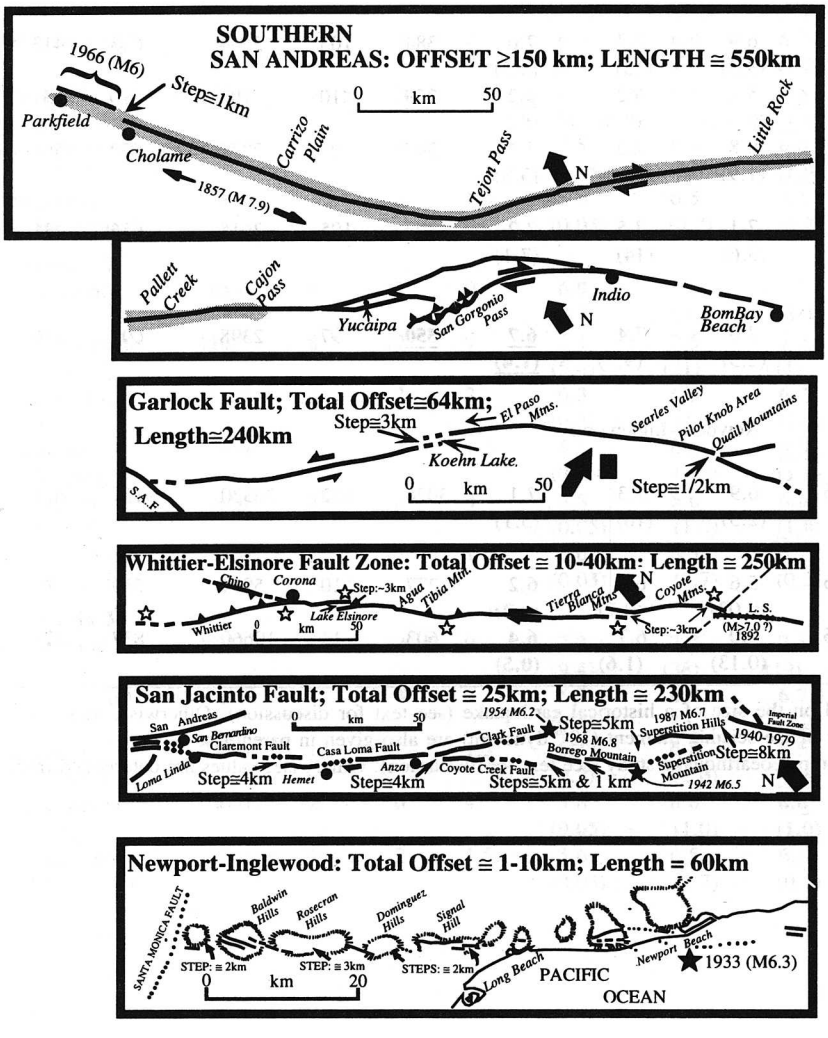

Figure 5. Strip maps showing surface traces of major strike-slip faults in southern California. The extent of the 1857 San Andreas earthquake is stippled. Epicenters of the 1933 Newport–Inglewood earthquake and the 1942 Santa Rosa and 1954 Salada Wash earthquakes along the San Jacinto are labeled by solid stars. The Borrego Mountain and Superstition Hills segments of the San Jacinto fault zone ruptured in 1968 and 1987, respectively. Locations of large steps (≧1 km) in fault trace are labeled. References to measures of cumulative geological offset are summarized in Wesnousky (1988). See text for further discussion.

ing northward from the fault toward Santa Monica. The consequences of these assumptions, when interpreted within the framework of equations 2 and 3, are summarized in Table 1 and plotted in Figure 6 along with the CIT-USGS data set. Thus, for example, in the plot labeled scenario 1 in Figure 6a, the solid diamond represents the preferred estimates of M_w and T resulting from the use of equation 2, the small open diamonds about the large solid triangle mark the range of values obtained with the use of equation 3, and the open circles represent the seismicity recorded by the CIT-USGS catalog since 1932. The two solid diamonds in the plot labeled sce-

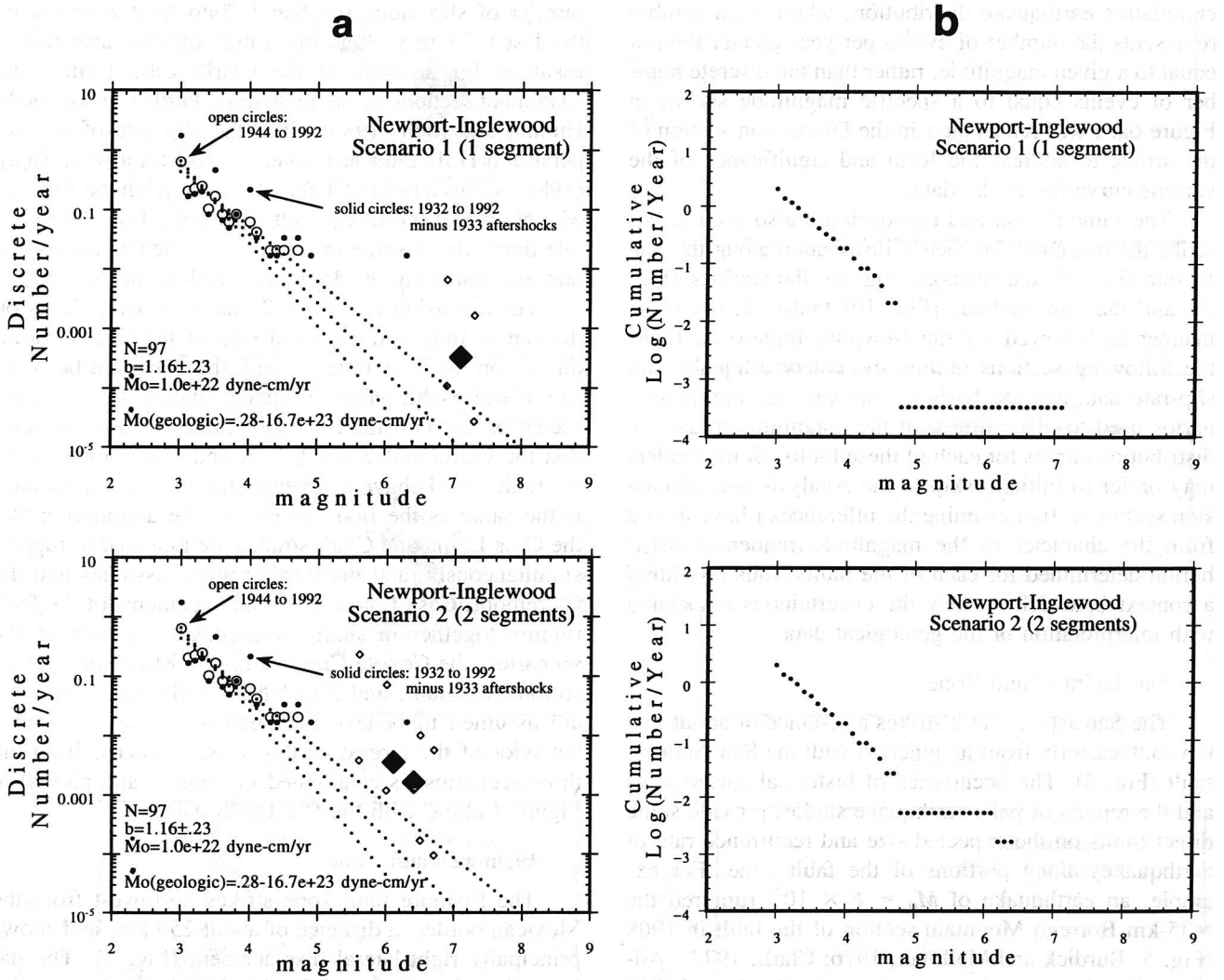

Figure 6. (a) Discrete number of events per year versus magnitude for the Newport–Inglewood fault. Open and closed circles represent the instrumental record of seismicity for the period 1944 to 1992 and 1932 to 1992, respectively. The dotted lines represent the 95% confidence limits on fit of the data for the period 1944 to 1992 to the equation $\log n = a - bM$, where n equals the number of events per year greater than or equal to magnitude M. The value b is determined via the maximum-likelihood method and the productivity a is defined by the total number of events recorded during the period. The total number of events (N), the b value and 95% confidence limits, and the seismic moment rate for the period 1944 to 1992 are listed in the lower left of each plot. Also listed in the lower left of each plot are the bounds on seismic moment rate determined from the fault slip rate data [$\dot{M}_0$ (geologic)]. Preferred (solid diamonds) and bounding estimates (open diamonds) of magnitude and recurrence rate of the largest expected earthquakes are determined from interpretation of geological data for two assumed rupture scenarios. The instrumental record (open symbols) and preferred geological estimates (solid diamonds) are combined to construct cumulative magnitude-frequency distributions (solid dots) in (b) for the respective rupture scenarios.

nario 2 (Fig. 6a) represent the preferred behavior of the two segments assumed for the second scenario, and again, the small diamonds show the range of values predicted for each with equation 3. In Figure 6b, the preferred estimates of M_w and T resulting from the use of equation 2, for each of the two scenarios, are further combined with the historical data and replotted in the form of a cumulative earthquake distribution, where each symbol represents the number of events per year greater than or equal to a given magnitude, rather than the discrete number of events equal to a specific magnitude shown in Figure 6a. I will return later in the Discussion section of the article to address the form and significance of the various curve-fits to the data.

The same format and approach are also used to describe the magnitude-frequency distribution along the San Jacinto (Fig. 7), the Elsinore (Fig. 8), the Garlock (Fig. 9), and the San Andreas (Fig. 10) faults. In the same manner as followed for the Newport–Inglewood fault, the following sections outline the paleoearthquake and slip-rate data and the basis for the various rupture scenarios used to place limits on the magnitude-frequency distribution curves for each of these faults. Some readers may prefer to initially skip to the Analysis and Discussion section to first examine the inferences I have drawn from the character of the magnitude-frequency distribution determined for each of the faults, thus providing a context in which to view the uncertainties associated with interpretation of the geological data.

San Jacinto Fault Zone

The San Jacinto fault strikes a distance of about 230 km southeasterly from its junction with the San Andreas fault (Fig. 5). The occurrence of historical earthquakes and the reports of paleoearthquake studies provide some direct limits on the expected size and recurrence rate of earthquakes along portions of the fault zone. For example, an earthquake of $M_0 \approx 1 \times 10^{26}$ ruptured the ≈35-km Borrego Mountain section of the fault in 1968 (Fig. 5, Burdick and Mellman, 1976; Clark, 1972). Additionally, the recurrence rate of events like that of 1968 was determined from study of trench exposures to be between 100 and 200 yr-during the last millennia (Clark *et al.*, 1972; Sharp, 1981). Similarly, in 1987, the ~30-km-long Superstition Hills section of the fault ruptured in an earthquake of $M_0 \approx 1 \times 10^{26}$ (Bent *et al.*, 1989; Magistrale *et al.*, 1989), and geomorphic and trenching studies place the average return time of similar events at between 150 and 300 yr (Hudnut and Sieh, 1989; Lindvall *et al.*, 1989). It is these values that are used to characterize the long-term behavior of the Borrego Mountain and Superstition Hills fault segments. Limits on the recurrence behavior of the remainder of the fault zone are obtained from equations 2 and 3, with the additional constraint that Klinger and Rockwell (1989) interpret structural and stratigraphic relations exposed in trenches to place a maximum recurrence interval of 250 yr for surface-rupturing events near Anza.

Rockwell's *et al.*'s (1990) study of displaced Holocene alluvial fan and fluvial deposits indicates that the slip rate of the fault at the latitude of Anza has averaged 9.2 ± 2 mm/yr during the last 9500 yr. Also near Anza, Sharp (1981) placed a similar minimum limit of 8 to 12 mm/yr of slip along the San Jacinto fault zone during the last 0.73 m.y. It is this range of slip rates that is assumed for analysis of the Clark, Casa Loma, and Claremont sections of the fault zone. Further to the south, Hudnut and Sieh (1989) place the slip rate of the Superstition Hills fault at between 2 and 6 mm/yr. Sharp (1981) places a limit of 1.6 to 2.2 mm/yr on the Borrego Mountain section of the fault during the last 6000 yr; a rate that I also assume to characterize the Coyote Mountain and Superstition Mountains sections of the fault.

Toward using equations 2 and 3 to place limits on the repeat time and expected size of the largest earthquakes on those sections of fault that have not been the site of successful paleoearthquake studies, three rupture scenarios are considered. The initial scenario assumes that the Claremont, Casa Loma, and Clark segments of the fault zone behave independently; the second scenario is the same as the first, except for the assumption that the Casa Loma and Clark strands are assumed to rupture simultaneously; and the third scenario assumes that the Claremont, Casa Loma, and Clark segments of the fault rupture together in single earthquakes. In each of the scenarios, the Coyote Creek, Borrego Mountain, Superstition Mountain, and Superstition Hills fault segments are assumed to behave independently. The recurrence behavior of the largest earthquakes, predicted from the three scenarios, is catalogued in Table 1 and plotted in Figure 7 along with the CIT-USGS data set.

Elsinore Fault Zone

The Elsinore fault zone strikes northwest from the Mexican border, a distance of about 250 km, and shows principally right-lateral displacement (Fig. 5). The paleoearthquake studies of Rockwell *et al.* (1985, 1986) indicate a maximum earthquake recurrence interval for surface-rupturing events equal to 250 yr at a site between Corona and Lake Elsinore. Toppozada and Parke (1982) interpret isoseismal data to indicate that a magnitude six event occurred along the same section of the fault in May 1910, and Brake (1987) and Brake and Rockwell (1987) reported the observation of a 50-cm displacement of a flume as evidence in support of the Elsinore being the source of that 1910 earthquake. They further suggested on that basis that M 6 to 6.5 earthquakes characterized the section of the fault between Corona and Lake Elsinore on average each 250 yr. There exists geomorphic expression of multiple 80- to 185-cm Holocene offsets within the Coyote Mountains further to the south (Rockwell *et al.*, 1986), an observation that led Pinault and

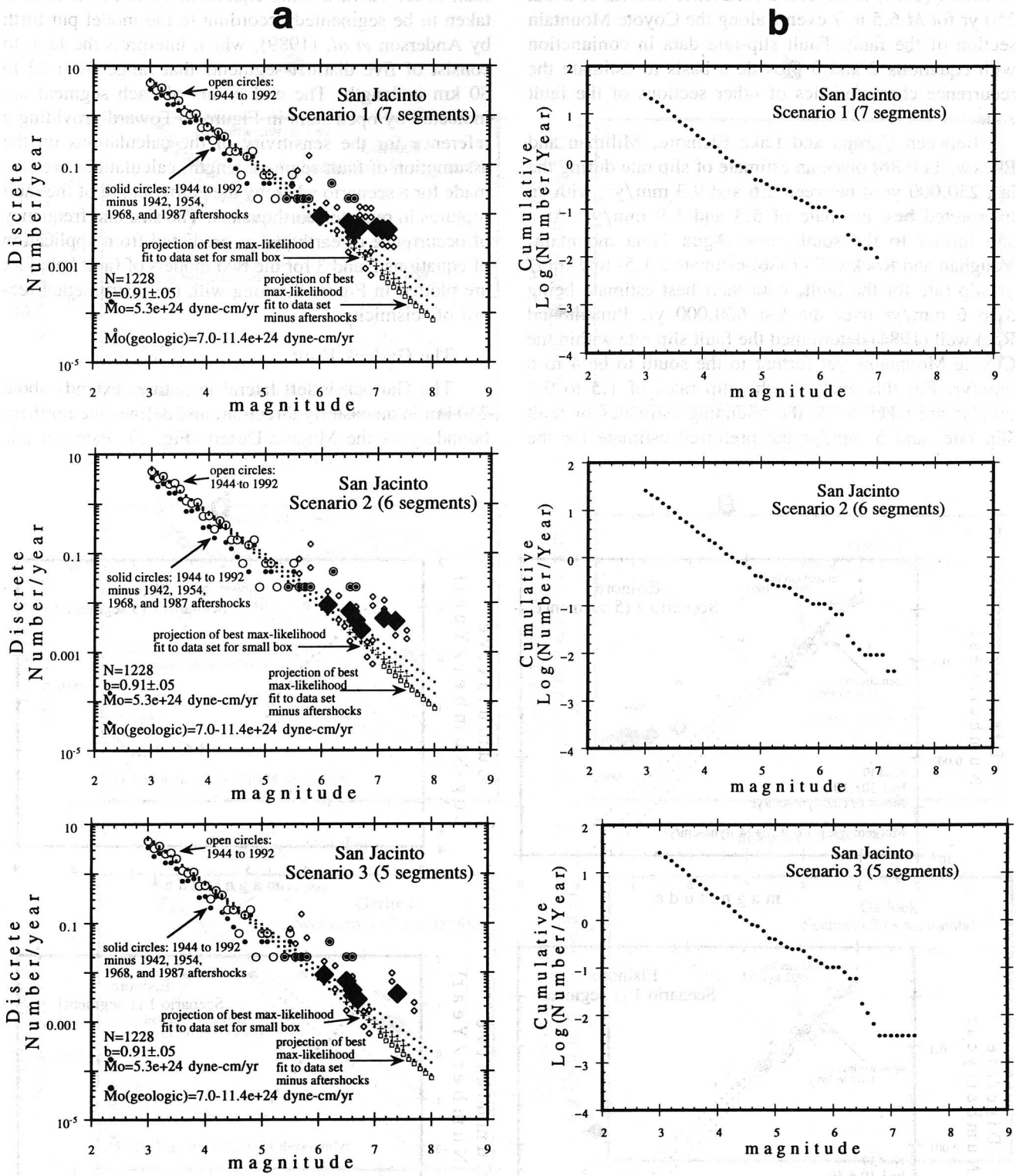

Figure 7. (a) Discrete and (b) cumulative number of events per year versus magnitude for the San Jacinto fault zone. The format is the same as Figure 6, except that solid circles represent activity during period 1944 to 1992 minus the aftershock distributions of large earthquakes along the fault during 1942, 1954, 1968, and 1987. The projection of the best maximum-likelihood fit to the data set, excluding the aftershock distributions, is also shown. See text for further discussion.

Rockwell (1984) to suggest a recurrence interval of about 350 yr for M 6.5 to 7 events along the Coyote Mountain section of the fault. Fault slip-rate data in conjunction with equations 2 and 3 provide a basis to estimate the recurrence characteristics of other sections of the fault zone.

Between Corona and Lake Elsinore, Millman and Rockwell (1986) place an estimate of slip rate during the last 250,000 yr at between 2.6 and 9.3 mm/yr, with an interpreted best estimate of 5.3 and 5.9 mm/yr. At a site further to the south, near Agua Tibia mountain, Vaughan and Rockwell (1986) estimate a 1.5- to 7-mm/yr slip rate for the fault, with their best estimate being 3 to 6 mm/yr over the last 600,000 yr. Pinault and Rockwell (1984) determined the fault slip rate within the Coyote Mountains yet further to the south to be 4 to 6 mm/yr. For this analysis, the slip rates of 1.5 to 9.3 mm/yr are taken to be the bounding estimates of fault slip rate, and 5 mm/yr the preferred estimate for the fault zone. Toward using equations 2 and 3, the fault is taken to be segmented according to the model put forth by Anderson *et al.* (1989), which interprets the fault to consist of five distinct segments that range from 22 to 80 km in length. The end points of each segment are indicated by open stars in Figure 5. Toward providing a reference for the sensitivity of the calculations on the assumption of fault segment length, calculations are also made for a scenario whereby the entire length of the fault ruptures in repeated earthquakes. The size and frequency of occurrence of earthquakes predicted from application of equations 2 and 3 for the two models of fault behavior are plotted in Figure 8, along with the instrumental record of seismicity.

The Garlock Fault

The Garlock is left lateral in nature, extends about 240 km in an easterly direction, and defines the northern boundary of the Mojave Desert (Fig. 5). Paleoseismic

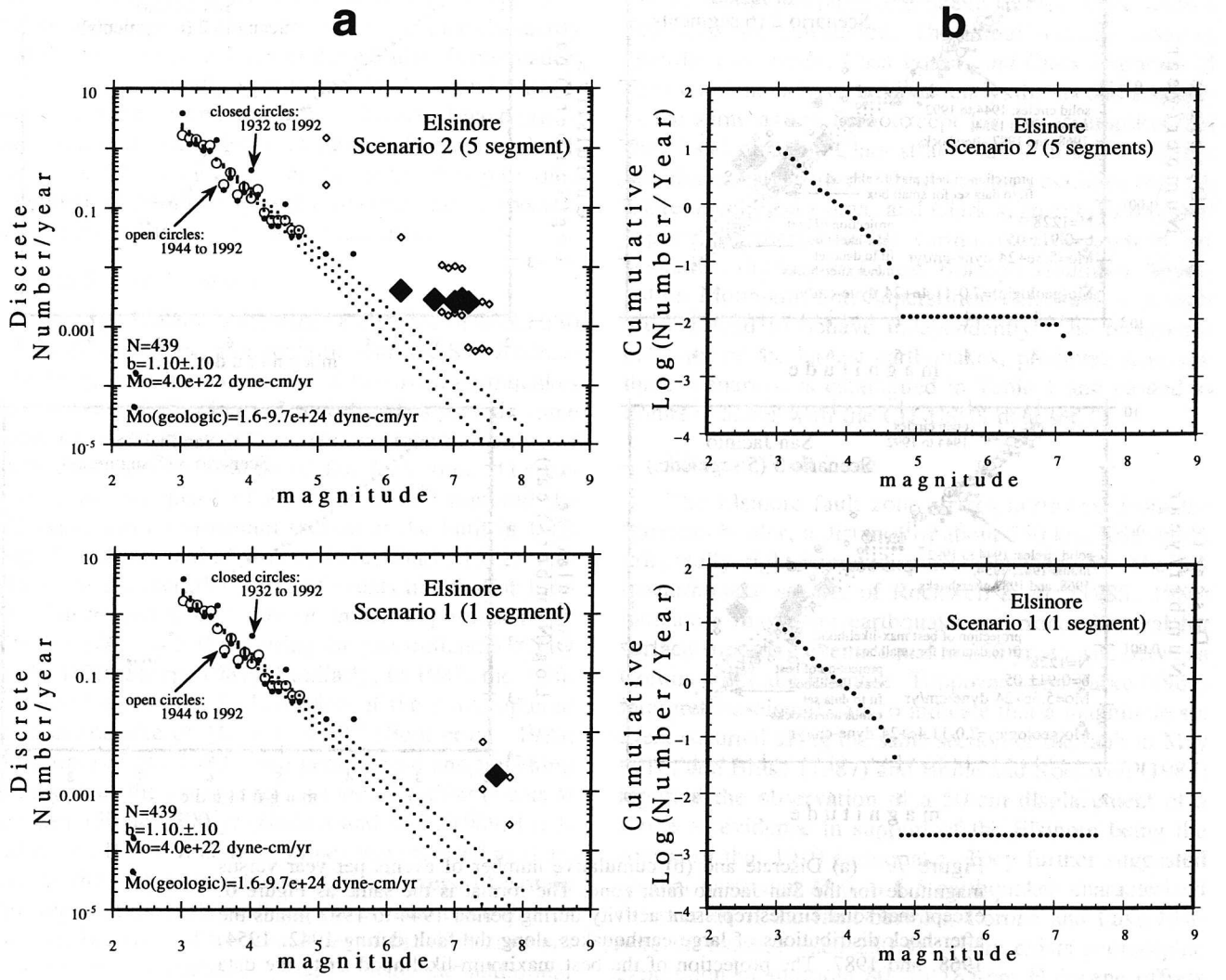

Figure 8. (a) Discrete and (b) cumulative number of events per year versus magnitude for the Elsinore fault zone. Same format as Figure 6.

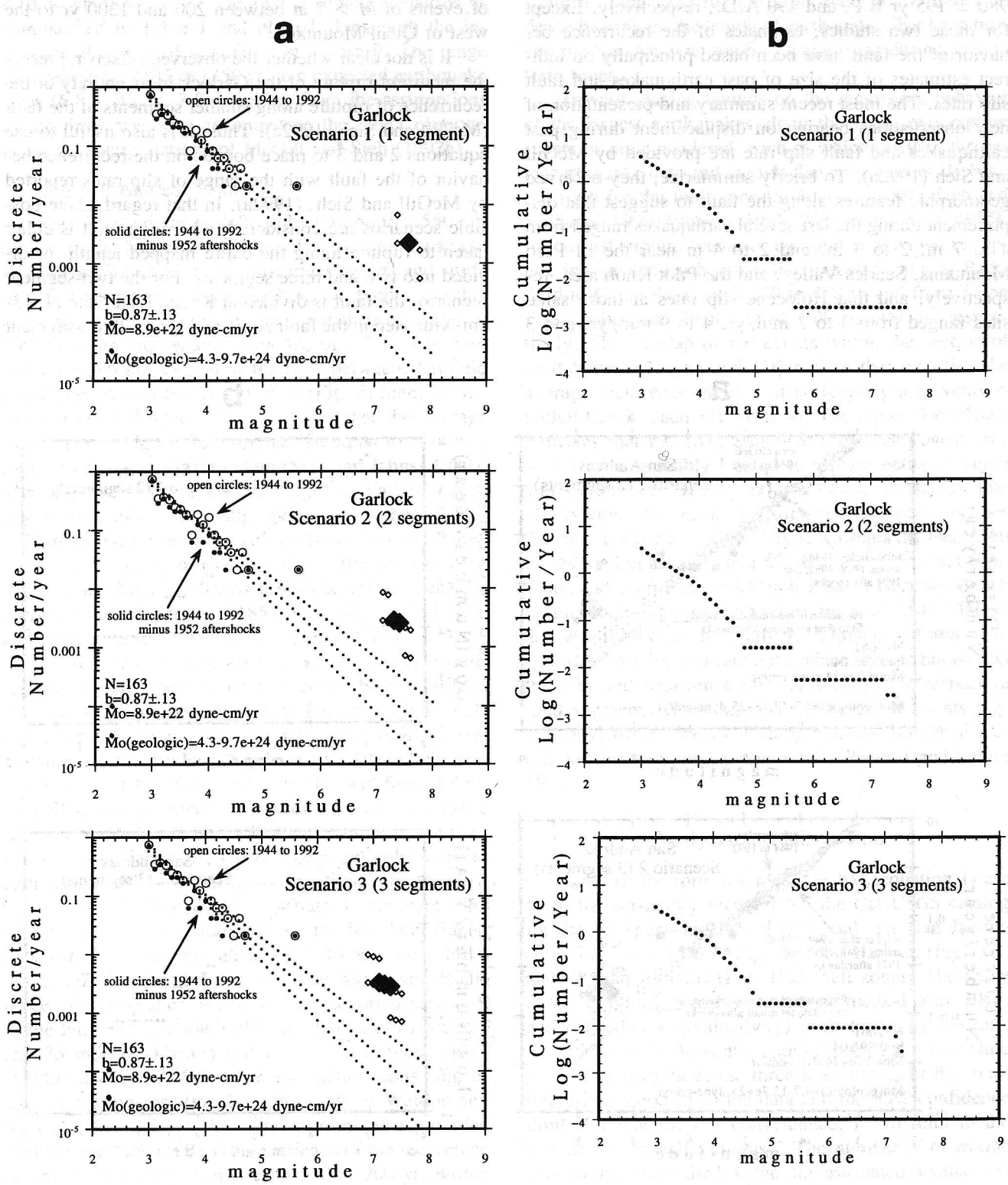

Figure 9. (a) Discrete and (b) cumulative number of events per year versus magnitude for the Garlock fault zone. Same format as Figure 6.

investigations to the west and east of Koehn Lake indicate that maximum ages of surface-rupture events equal 980 ± 195 yr B.P. and 490 A.D., respectively. Except for those two studies, estimates of the recurrence behavior of the fault have been based principally on indirect estimates of the size of past earthquakes and fault slip rates. The most recent summary and presentation of new observations bearing on displacement during past earthquakes and fault slip rate are provided by McGill and Sieh (1992a). To briefly summarize, they observed geomorphic features along the fault to suggest that displacement during the last several earthquakes ranged from 4 to 7 m, 2 to 3 m, and 2 to 4 m near the El Paso Mountains, Searles Valley, and the Pilot Knob area, respectively, and that Holocene slip rates at those same sites ranged from 4 to 7 mm/yr, 4 to 9 mm/yr, and 3 to 9 mm/yr. Dividing the observed offsets by the range of slip rates led them to estimate the recurrence interval of events of $M > 7$ at between 200 and 1300 yr to the west of Quail Mountain.

It is not clear whether the observed offsets represent the recurrent rupture of the Garlock in its entirety or the recurrence of rupture along smaller segments of the fault (McGill and Sieh, 1992a). Thus, it is also useful to use equations 2 and 3 to place bounds on the recurrence behavior of the fault with the range of slip rates reported by McGill and Sieh, (1992a). In that regard, three possible scenarios are considered, where the fault is either taken to rupture along the entire mapped length, or divided into two and three segments. For the two-segment scenario, the fault is divided at Koehn Lake, site of a 3-km-wide step in the fault zone, and for the three-segment

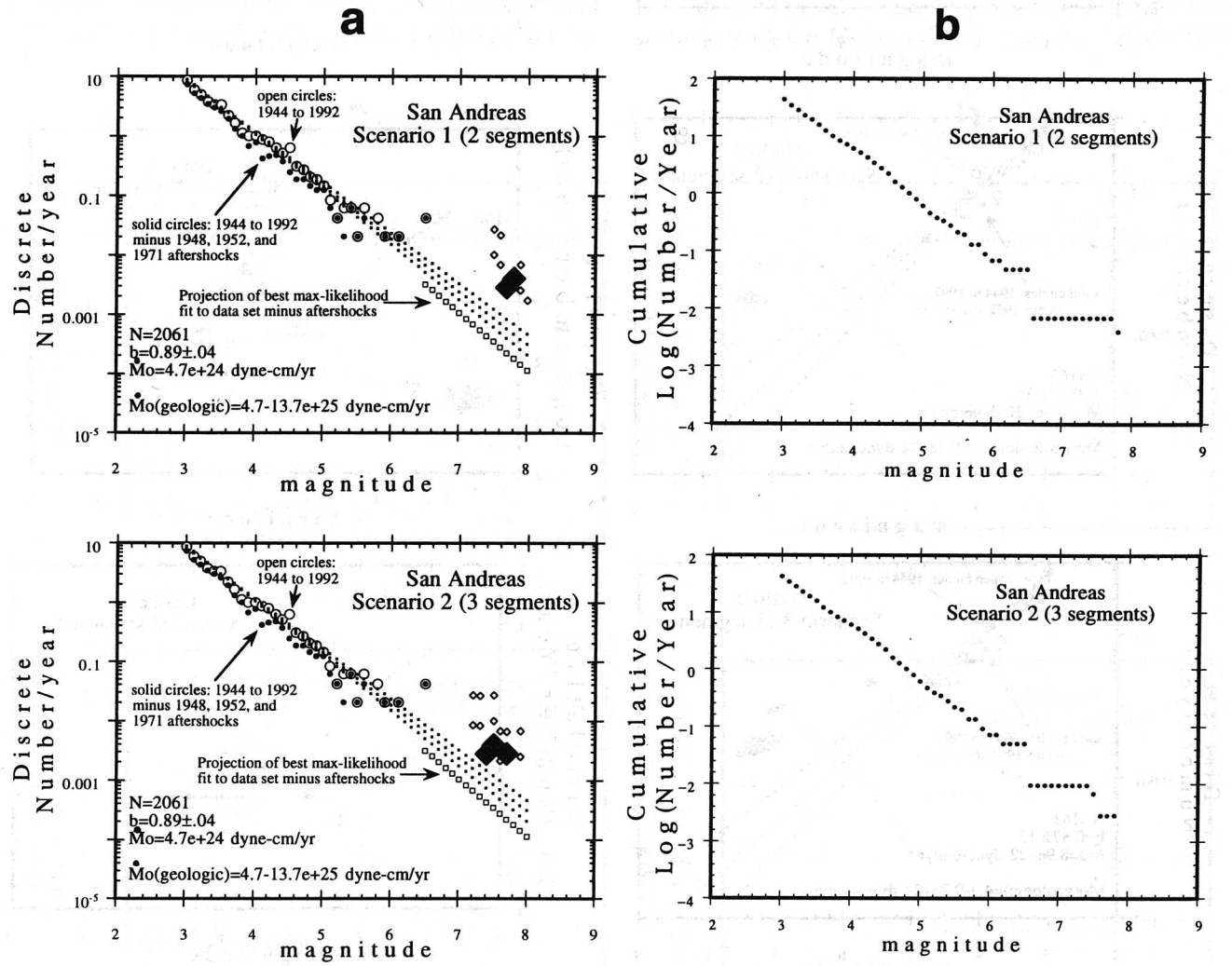

Figure 10. (a) Discrete and (b) cumulative number of events per year versus magnitude for the San Andreas fault zone. Same format as Figure 6, except that solid circles represent activity during the period 1944 to 1992 minus the aftershock distributions of large earthquakes near the fault during 1948, 1952, and 1971. The projection of the best maximum-likelihood fit to the data set, excluding the aftershock distributions, is also shown. See text for further discussion.

model the segments are arbitrarily taken at 60, 80, and 100 km. The recurrence behavior of the largest earthquakes predicted from the two assumed scenarios is summarized in Table 1 and plotted along with the instrumental record of seismicity in Figure 9. The range of repeat times (105 to 1350 yr) and expected earthquake sizes ($6.8 < M_W < 7.8$) resulting from the assumptions of the three scenarios encompasses the direct observations and interpretations of McGill and Sieh (1992b).

The San Andreas Fault

The San Andreas is defined here to be that 550-km section of the fault that strikes southward from Parkfield to Bombay Beach (Fig. 5). Historical reports and study of offset geomorphic features along the fault show that an earthquake of seismic moment equal to 53 to 90 $\times$ 10^{26} dyne-cm, equivalent to an M_W of 7.7 to 7.9, ruptured a ~380-km section of the fault between Parkfield and Cajon Pass in January of 1857 (Fig. 5; Sieh, 1978). The offset of Wallace Creek requires that the average rate of slip along the San Andreas be equal to ~34 $\pm$ 3 mm/yr within the Carrizo Plain (Sieh and Jahns, 1984). The offset of small gullies adjacent to Wallace Creek also records evidence of slip ranging from about 9.5 to 12.3 m during the last three earthquakes (Sieh and Jahns, 1984). Dividing the offsets recorded in the gullies by the slip rate led Sieh and Jahns (1984) to estimate the recurrence period between 1857-type (M_W = 7.7–7.9) earthquakes to range between 240 and 450 yr.

There also exist paleoearthquake and slip-rate studies farther south along the fault. Reported bounds on fault slip rate at points between Tejon Pass and Cajon Pass range between 16 and 43 mm/yr (Prentice *et al.*, 1988; Salyards *et al.*, 1987; Salyards *et al.*, 1991; Schwartz and Weldon, 1987; Sieh, 1984; Weldon and Sieh, 1985). At Pallett Creek, trench exposures indicate an average recurrence interval of about 130 yr for surface-rupturing earthquakes (Sieh *et al.*, 1989). The geomorphic expression of repeated 2- to 4-m offsets in the vicinity of Pallett Creek (Sieh, 1978) and surface rupture in the great 1857 (M_W = 7.7 to 7.9) earthquake and the San Juan Capistrano (M_W = 7.5) earthquake of 1812 (Jacoby *et al.*, 1988; Sieh, 1978) at the Pallett Creek site reflect the recurrence of earthquakes of $M_W > 7.5$. Reported estimates of the fault slip rate south of Cajon Pass are between 11 and 35 mm/yr (Harden and Matti, 1989; Sieh, 1986; Weldon and Sieh, 1985) with the tightest constraint of 24 $\pm$ 4 mm/yr resulting from the study of Weldon and Sieh (1985) at Cajon Pass. Excavations also provided Weldon and Sieh (1985) with evidence of the recurrence of ground-rupturing events, each 150 to 200 yr, within Cajon Pass. Yet, farther to the south, near Indio, Sieh and Williams (1990) place the recurrence of large earthquakes at every 2 to 3 centuries. There are reports of 1- to 4-m offsets of young geomorphic features at sites along the reach of the San Andreas south of Cajon Pass that reflect prehistoric earthquake displacements (Keller *et al.*, 1982; Sieh, 1978; Weldon and Sieh, 1985), but, in contrast to the 1857 rupture zone, there is no direct evidence bearing on the length of earthquakes that have broken the San Andreas south of Cajon Pass during prehistoric times.

Toward placing bounds on the recurrence behavior of the largest earthquakes along the fault, two rupture scenarios are considered, each of which satisfies the paleoearthquake data and models that have previously been put forth for the fault zone (Sieh *et al.*, 1989; Sieh and Williams, 1990; Weldon, 1991; Weldon and Sieh, 1985). In the first rupture scenario, the fault is assumed to rupture in repeated earthquakes that extend from near Parkfield to Cajon Pass, each 250 to 450 yr and from Tejon Pass to Bombay Beach, each 200 to 300 yr, respectively. The overlap of the events within the section of fault between Tejon and Cajon Pass then satisfies the average recurrence interval of surface-rupture events at Pallett Creek, each 130 yr or so. The reported evidence indicates that the 1812 San Juan Capistrano event (M_W = 7.5) was probably limited to rupture between Tejon and Cajon Pass (Jacoby *et al.*, 1988). To satisfy that observation, the second rupture scenario again assumes the repeated rupture of 1857-type earthquakes, each 250 to 450 yr, but assumes that the sections of the fault from Tejon to Cajon Pass and Cajon Pass to Bombay Beach rupture independently with return times of 250 to 450 yr and 200 to 300 yr, respectively. Equations 2 and 3, in conjunction with slip-rate data, place further bounds on the size and recurrence of events along the respective fault segments. The size and frequency of events predicted by these scenarios, along with the historical record of seismicity, are summarized in Table 1 and Figure 10.

Analysis and Discussion

Lines of the form $\log n = a - bM$ (equation 1) are fit to the seismicity recorded by the CIT-USGS catalog for the Newport–Inglewood (Fig. 6a), the San Jacinto (Fig. 7a), the Elsinore (Fig. 8a), the Garlock (Fig. 9a), and the San Andreas (Fig. 10a) fault zones. The value of b is fit by the maximum likelihood method (Aki, 1965) and the value a (productivity) is fit to satisfy the total number of $M > 3$ events reported during the recording period. In each case, the three lines represent the maximum-likelihood fit to the data and the 95% confidence limits for that fit. For convenience, I will refer to the line fits as "b-value curves." The number N of events used to determine the b value, the estimated b value and 95% confidence limits, and the seismic moment release rate $\dot{M}_0$ for the period 1944 to 1992 are listed in the lower left of each of the plots. For comparison and later discussion, the bounds on the seismic moment rate $\dot{M}_0^g$ placed on each fault by observations of fault slip rate are also

listed in the lower left of each plot. The bounding values of $\dot{M}_0^g$ reflect directly the range of slip rates reported for each fault in Table 1.

The recurrence estimates for the largest expected earthquakes arising from interpretation of the geological data fall well above projections of the b-value curves for the Elsinore (Fig. 8a), Garlock (Fig. 9a), and San Andreas (Fig. 10a) fault zones. In the case of the Newport–Inglewood fault, overlap in geological estimates and the b-value curves exists, but the overlap is slight and occurs only for the extreme lower bounds placed by geology on the earthquake recurrence rate (return times > 10,000 yr) for the largest earthquakes expected along the fault (Fig. 6a). Preferred recurrence estimates along the Newport–Inglewood arising from geological observations fall well above the 95% confidence limits of the projected b-value curves. It is only along the San Jacinto fault that the geological estimates of recurrence show a clear overlap with projections of the b-value curves determined from the instrumental record (Fig. 7).

The same result may be illustrated in another manner. I have plotted in Figure 11 the ratio of the recurrence rate of earthquakes predicted from the geological data (i.e., equations 2 and 3) to that predicted from extrapolation of the maximum-likelihood fit to the historical data for each fault and rupture scenario. Thus, in Figure 11, each column of data represents a specific rupture scenario for a fault zone. The solid diamonds are the ratio of the preferred values of recurrence rate for the respective segments in each scenario to the recurrence rate predicted from the maximum-likelihood fit to the historical data at the same magnitude. The open triangles represent the same ratio for the bounding values of recurrence rate and expected magnitude determined from equation 3 for the respective rupture scenarios for each fault zone. The plot (Fig. 11) illustrates that estimates of the recurrence rate of the largest expected earthquakes along the Newport–Inglewood, Elsinore, Garlock, and San Andreas faults, arising from interpretation of geological data, are minimally two to three times to more than an order of magnitude greater than predicted by extrapolating the maximum-likelihood fit to the instrumental record of seismicity. In contrast, the geologic estimates of the recurrence rate for the San Jacinto spans the rate (ratio = 1) predicted from extrapolation of earthquake statistics.

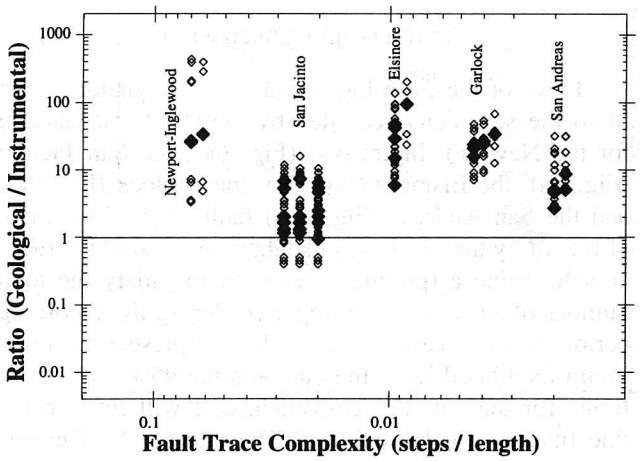

Figure 11. Ratio of the recurrence rate of earthquakes predicted from geological data to that predicted from extrapolation of the maximum-likelihood fit of equation 1 to the instrumental record of seismicity versus fault trace complexity. See text for further explanation.

Similarly, differences in the character of earthquake recurrence are also seen when the preferred geological recurrence estimates are combined with the instrumental record of seismicity to construct cumulative earthquake frequency distributions for each fault zone. For example, along the San Jacinto fault zone (Fig. 7b), the number of events N for any given rupture scenario decreases relatively smoothly as a function of magnitude to some maximum value of magnitude, consistent with the Gutenberg–Richter model of earthquake behavior. In contrast, the cumulative distributions along the Newport–Inglewood (Fig. 6b), the Elsinore (Fig. 8b), the Garlock (Fig. 9b), and the San Andreas (Fig. 10b) fault zones show a shape that would be predicted by the characteristic earthquake model (Fig. 1b).

The use of equations 2 and 3 assumes that the entire moment rate along faults or fault segments is released solely by earthquakes of maximum magnitude. Thus, some concern may arise that I have underestimated the recurrence times of the maximum expected events because the contribution to slip rate represented by the occurrence of lesser-sized events observed during the instrumental record of recording is not considered. The sum seismic moment ΣM_0^{sm} due to smaller events during the recurrence time T of one maximum expected event may be defined to equal $\dot{M}_0^{sm} \times T$, where $\dot{M}_0^{sm}$ is the seismic moment rate due to events of size less than the expected maximum-size event of seismic moment M_0^e. If lesser-sized events during the recurrence of the expected maximum-size event M_0^e do accommodate a portion of the fault slip rate, then it may be argued (e.g., Wesnousky *et al.*, 1983) that the expected recurrence time T of M_0^e should be written $T = (M_0^e + \Sigma M_0^{sm})/\dot{M}_0^g$ which, in turn, can be rewritten as $T = (M_0^e/\dot{M}_0^g)/(1 - (\dot{M}_0^{sm}/\dot{M}_0^g))$. The expression is equal to equations 2 and 3 if $\dot{M}_0^{sm}$ is zero. If $\dot{M}_0^{sm}$ is nonzero, then the use of equations 2 and 3 will underestimate the return time of the largest expected events.

Bounds on the geologically determined seismic moment rate are listed along with the seismic moment rate determined from the instrumental period of recording for the Newport, San Jacinto, Elsinore, Garlock, and San Andreas faults in Figures 6 through 10, respectively. The ratios $\dot{M}_0^{sm}/\dot{M}_0^g$ for the Newport–Inglewood (0.006 to 0.3),

Elsinore (0.004 to 0.03), Garlock (0.009 to 0.02), and San Andreas (0.03 to 0.1) faults are very small. Thus, whether or not the seismic moment contribution of small events is included in estimates of T, the observations show that the preferred recurrence estimates of the largest expected earthquakes derived for the geological data fall above the projections of the b-value curves for the Newport, Elsinore, Garlock, and San Andreas faults. In contrast, ignoring the ratio $\dot{M}_0^{sm}/\dot{M}_0^g$ for the San Jacinto fault (0.46 to 0.75) may lead to underestimates by a factor of 2 to 4 of the return time of maximum expected events. The sense of potential error would generally strengthen the observation that geological estimates of recurrence overlap with projections of the b-value curves along the San Jacinto fault. Hence, with respect to the observations put forth in the preceding paragraphs, it is not significant whether or not the smaller events are included in the estimates of return time for the maximum expected events along the fault zone. Furthermore, the ratios $\dot{M}_0^{sm}/\dot{M}_0^g$ calculated for the faults represent maximum values. For example, the M 6.0 event of 1937 and the M 6.2 Elmore Ranch earthquake contribute significantly to the instrumentally determined seismic moment rate for the San Jacinto fault, but occurred on faults striking near perpendicular to the San Jacinto fault. Similarly, the 1952 Kern County earthquake sequence contributes to the observed seismic moment rate along the San Andreas and Garlock faults, but most certainly did not contribute to slip directly along either of the two faults. Moreover, when viewing seismicity along the fault zones (e.g., Fig. 2), it is clear that most of the smaller earthquakes do not occur directly on the fault trace, but in the zone around it. Although the scatter in locations may in part reflect nonvertical fault dips and errors in event location, it seems clear that not all of the events, and perhaps even a minority, are contributing to the offset that is measured by geologists along fault traces and used to determine fault slip rate. And finally, with respect to this study, it is useful to recall that paleoearthquake studies have been used in a number of instances to place limits on the recurrence characteristics of the faults. This latter information is independent of estimates of fault slip rate.

Thus, to first order, when combining instrumental and geological data sets to define the shape of the magnitude-frequency distribution, it appears that seismicity along the Newport–Inglewood, Elsinore, Garlock, and San Andreas faults is more likely described by the characteristic earthquake distribution (Fig. 1b), whereas the Gutenberg–Richter distribution (Fig. 1a) provides a suitable description of seismicity along the San Jacinto fault. It is natural to seek a single model to explain or describe the character of seismicity along the fault zones. It might be argued that, over the course of an entire earthquake cycle, the seismicity along all faults satisfies the Gutenberg–Richter relationship of equation 1. If so, the characteristic earthquake distribution implied in Figures 6a, 8a, 9a, and 10a for the Newport–Inglewood, Elsinore, Garlock, and San Andreas faults must then be considered an artifact of a limited instrumental data set. The consequence of such an assertion is one of importance, for then the observations of Figures 6a, 8a, 9a, and 10a clearly require that seismicity during the recurrence interval between the largest earthquakes along a fault zone is not steady in time. The assertion is also of importance to seismic hazard analysis because it implies that the recurrence rate of the largest earthquakes along a fault zone may be severely underestimated if based on the extrapolations of historical earthquake statistics that are assumed to satisfy equation 1, a point that has been made previously (e.g., Allen *et al.*, 1965; Wesnousky *et al.*, 1983; Youngs and Coppersmith, 1985).

Conversely, it might be asserted that, over the long term, seismicity along all faults is most appropriately described by the characteristic earthquake distribution, in which case one must then assume that the rate of seismicity has been unusually high along the San Jacinto fault zone during the last 60 yr, and that the general agreement of geological estimates of return time with estimates derived from the extrapolation of historical seismicity via equation 1 is merely serendipitous. The observation that a number of $M > 6$ earthquakes have occurred along the San Jacinto during the period between 1944 and 1992 may lend credence to such a contention. Possibly the instrumental portion of the magnitude-frequency curve for the San Jacinto fault is dominated by aftershocks of these larger events. The San Jacinto fault zone produced the M 6.2 Salada Wash earthquake of 19 March 1954, the M 6.4 Borrego Mountain earthquake of 9 April 1968, and the M 6.2 and 6.6 earthquakes of October 1987 (Figs. 3 and 4). I have also plotted in Figure 7a the projection of the maximum-likelihood fit to the instrumental record of activity for the case where I have removed both the mainshock and all events in the catalog for a period of 1 yr after the origin time of the just-mentioned earthquakes along the San Jacinto fault zone; a period of time sufficient to remove the majority of the aftershock sequences for each of the events (Fig. 3). The resulting curve leads to the same result as found in the case when all events in the catalog are considered. That is to say, extrapolation of the curves intersects the field of data predicted from interpretation of the geological data, allowing the interpretation that the magnitude-frequency distribution may be fit by the Gutenberg–Richter distribution.

It might also be suggested that the Gutenberg–Richter distribution observed for the entire San Jacinto actually reflects the sum of seismicity along a number of separate fault segments, each of which displays a characteristic earthquake distribution. Indeed, both the geological and historical records show that the entire length of the fault zones considered here do not rupture their lengths in entirety during single earthquakes. Thus, to-

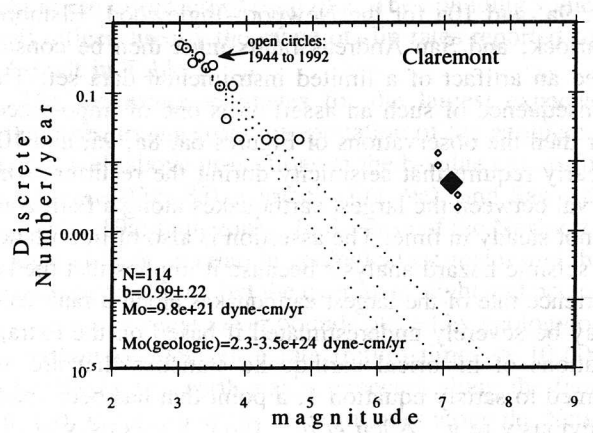

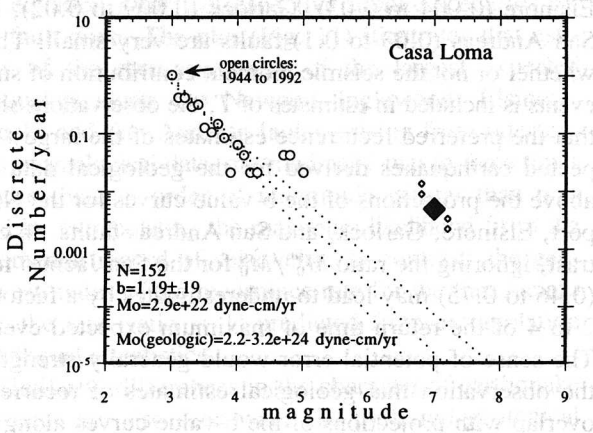

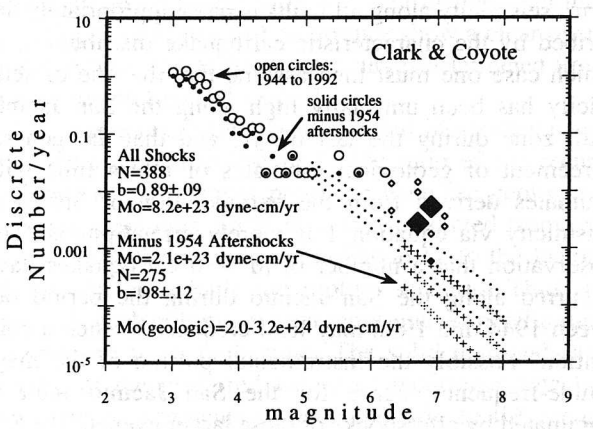

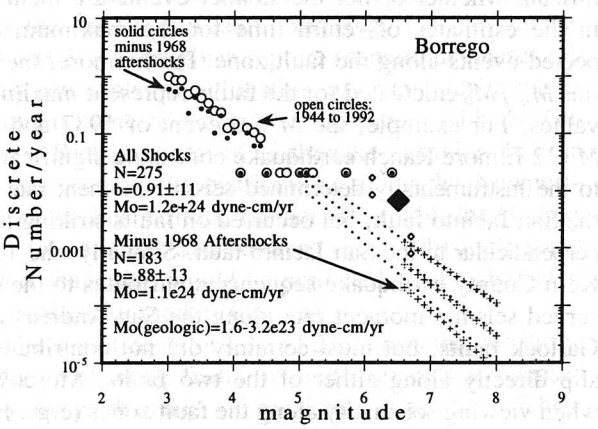

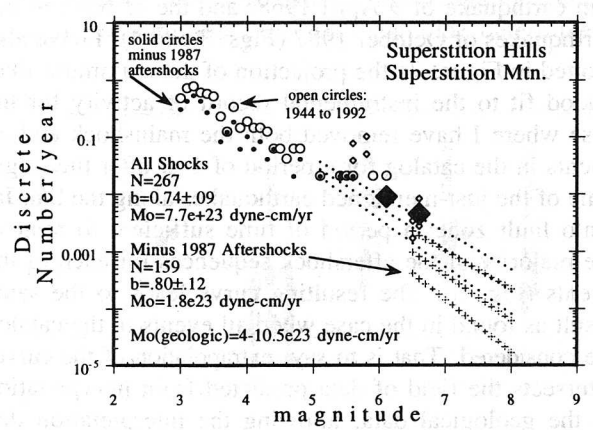

Figure 12. Discrete number of events per year versus magnitude for all shocks (open circles) and minus the aftershock distributions of $M > 6$ events (solid circles) for individual segments of the San Jacinto fault zone for the period 1944 to 1992 (open circles). Same format as Figure 6. The seismicity is selected from sections of the box around the San Jacinto shown in Figure 2b, which correspond to the length of individual fault segments that are marked in Figure 5. The maximum-likelihood and 95% confidence limits of the fit of a line of the form of equation 1 to the instrumental record of seismicity with (dotted line) and without aftershocks (lines of plus marks) are given for the period between 1944 and 1992. See text for further explanation.

ward examining this suggestion, I have used the same approach to define separately the magnitude-frequency distribution for the Claremont, Casa Loma, Clark and Coyote, Borrego, and Superstition Hills and Mountain segments of the San Jacinto fault zone in Figure 12. Estimates of the recurrence rate of the largest earthquakes obtained by extrapolation of the earthquake statistics are much less than predicted from analysis of the geological data for the Claremont and Casa Loma strands. In contrast, estimates of the repeat time of the largest earthquakes based on the two methods show overlap and allow the distributions to be characterized by the Gutenberg–Richter distribution along the Clark and Coyote, Borrego, and Superstition Hills segments of the fault. It is also these latter segments that produced major earthquakes during the instrumental period of recording, raising the possibility that the distributions for these faults are dominated by the aftershock distributions of the less frequent but large events that have occurred during the instrumental period of recording.

The *M* 6.5 Santa Rosa earthquake of 21 October 1954, the *M* 6.4 Borrego Mountain earthquake of 9 April 1968, and the *M* 6.2 and 6.9 earthquakes of November 1987 occurred along the Clark and Coyote, Borrego Mountain, and Superstition Hills segments of the San Jacinto fault zone, respectively (Fig. 5). The majority of aftershocks for those events are limited to the year subsequent to the mainshock. Figure 12 also shows the b-value curves determined for the data set where all events during the 1 yr subsequent to the respective mainshocks have been removed. Removal of aftershocks results in a marked decrease in the rate of seismicity predicted by extrapolation of the instrumental data for the Clark and Coyote and Superstition Hills segments. For all three fault segments, geological estimates of recurrence rate fall well above the maximum-likelihood b-value curve, although a small overlap of the extreme lowest bounds on recurrence rate placed by geological data with the 95% confidence limits on the b-value curves does remain for the Superstition Hills and Borrego segments. When viewed in this manner, the data permit the idea that the Gutenberg–Richter distribution observed for the entire San Jacinto (Fig. 7) reflects the sum of seismicity resulting from a number of separate fault segments, each of which displays a characteristic earthquake distribution when viewed independently.

In some earlier work, I noted that the faults considered here are not characterized by a single throughgoing fault trace, but rather, display a number of distinct steps in the fault trace (Wesnousky, 1988). The steps in the fault trace that measure $\geqq$1 km in width perpendicular to the fault strike are marked in Figure 5 and were the basis to define the complexity of each fault trace by the number of observed fault steps per unit length along the respective faults. I also suggested that the productivity of the faults was inversely proportional to fault trace complexity (Wesnousky, 1990). That result was based on the instrumental record between 1932 and 1992. Examination of Figure 3 shows that productivity along the Newport–Inglewood fault is dominated by an extended aftershock sequence associated with the 1993 Long Beach earthquake. If only the period between 1942 and 1992 is considered, the productivity for the Newport–Inglewood decreases markedly, in which case support is removed from the earlier suggestion that productivity for these five faults is inversely proportional to fault trace complexity. In Figure 11, I further plot, as a function of fault trace complexity, the ratio of the recurrence rate of earthquakes predicted from the geological data to that predicted from extrapolation of earthquake statistics for each respective fault and rupture scenario (for clarity of presentation, the data for each rupture scenario are slightly offset from each other). A relationship between fault trace complexity and the ratio is not observed and, hence, no clear link between the shape of the earthquake frequency distribution and fault trace complexity is evident.

It is reasonable to question the sensitivity of this analysis to the dimension of the box placed around each fault (Fig. 2). The width of the boxes is about 40 km for each fault, except for the Newport–Inglewood, where a box only 15-km wide is used to preclude inclusion of seismicity from the nearby Palos Verdes fault zone. With respect to the Elsinore (Fig. 8a), Garlock (Fig. 9a), and San Andreas (Fig. 10a), the choice of a thinner box width results in inclusion of fewer small and moderate earthquakes in the historical data. The effect would generally exacerbate the discrepancies between geological and statistical estimates of return time for the largest earthquakes along the fault zone. Thus, the observation that seismicity along these faults appears best described by a characteristic earthquake distribution seems robust. In contrast, the observation that the magnitude-frequency distribution may be described by the Gutenberg–Richter relation might be shown to be false if a reduction in box width leads to a significant reduction in the number of events in the catalog attributed to the San Jacinto fault zone. To allow inspection of the idea, I have also plotted in Figure 7a the projection of the best maximum-likelihood fit to the instrumental data set when only events within a 10-km-wide box centered on the fault zone are included. The width of the mapped fault zone itself approaches 10 km in places. The resulting curve does predict a lesser rate of occurrence for larger earthquakes, but not so much less that extrapolation of the line does not intersect the field of values predicted from the geological data.

Conclusions

When combining geological and instrumental data bearing on the size and repeat time of earthquakes along the major strike-slip fault zones of southern California

to place limits on the shape of the magnitude-frequency distribution, seismicity along the Newport–Inglewood, Elsinore, Garlock, and San Andreas faults is consistent with the characteristic earthquake model of fault behavior, whereas seismicity along the San Jacinto fault zone appears suitably described by the Gutenberg–Richter relationship. However, if attention is limited to segments of the San Jacinto that are separated by distinct steps in fault trace or the rupture zones of large historical earthquakes, the observed distribution along each segment may be explained by the characteristic earthquake model. The observation permits the interpretation that the Gutenberg–Richter distribution observed for the entirety of the San Jacinto reflects the sum of seismicity along a number of distinct fault segments, each of which displays a characteristic earthquake distribution. The limited period of instrumental data used here is insufficient to disprove an alternate hypothesis that all faults will display a Gutenberg–Richter distribution when averaged over the course of a complete earthquake cycle. But, given that (1) the last 5 decades of seismicity is the best indicator of the expected level of small to moderate-size earthquakes in the next 50 yr, and (2) it is generally about this period of time that is of interest in seismic hazard and engineering analysis, the answer to the question posed in the title of this article, at least when concerned with practical implementation of seismic hazard analysis, appears to be the "characteristic earthquake distribution."

Acknowledgments

Useful comments were provided by John Anderson, Yehuda Ben-Zion, and Yan Kagan in the early stages of this work. I thank Paul Reasenberg and Fred Klein for providing discussion and a computer code to check my b-value calculations. The research was supported by NSF Grant Number EAR-9005092 and SCEC Grant Number 1-1-334-5308-827. Center for Neotectonics Contribution Number 11.

References

Aki, K. (1965). Maximum likelihood estimates of b in the formula $\log N = a - bM$ and its confidence limits, *Bull. Earthquake Res. Inst.* **43**, 237–239.

Aki, K. and P. G. Richards (1980). *Quantitative Seismology: Theory and Methods*, W. H. Freeman, San Francisco, California, 1–932.

Allen, C. R., P. St. Amand, C. F. Richter, and J. M. Nordquist (1965). Relationship between seismicity and geological structure in the southern California region, *Bull. Seism. Soc. Am.* **55**, 753–797.

Anderson, J. G. (1979). Estimating the seismicity from geological structure for seismic-risk studies, *Bull. Seism. Soc. Am.* **69**, 135–158.

Anderson, J. G., T. K. Rockwell, and D. C. Agnew (1989). Past and possible future earthquakes of significance to the San Diego region, *Earthquake Spectra* **5**, 289–335.

Benioff, H. (1938). The determination of the extent of faulting with application to the Long Beach earthquake, *Bull. Seism. Soc. Am.* **69**, 135–158.

Bent, A. L., D. V. Helmberger, R. J. Stead, and P. Ho-Liu (1989). Waveform modeling of the November 1987 Superstition Hills earthquakes, *Bull. Seism. Soc. Am.* **79**, 500–513.

Bird, P. and R. Rosenstock (1984). Kinematics of present crust and mantle flow in southern California, *Geol. Soc. Am. Bull.* **28**, 77–84.

Brake, J. F. (1987). Analysis of historic and pre-historic slip on the Elsinore Fault at Glen Ivy Marsh, Temescal Valley, Southern California, *Master's Thesis*, San Diego State University, San Diego, 103 pp.

Brake, J. F. and T. K. Rockwell (1987). Magnitude of slip from historical and prehistorical earthquakes on the Elsinore fault, Glen Ivy Marsh, southern California (abstracts with programs), *Geol. Soc. Am.* **19**.

Burdick, L. and G. R. Mellman, (1972). Inversion of the body waves from the Borrego Mountain earthquake to source mechanism, *Bull. Seism. Soc. Am.* **66**, 1485–1499.

Clark, M. M. (1972). Surface rupture along the Coyote Creek fault, the Borrego Mountain earthquake of April 9, 1968, *U.S. Geol. Surv. Profess. Pap. 787*, 55–86.

Clark, M. M., A. Grantz, and M. Rubin (1972). Holocene activity of the Coyote Creek fault as recorded in sediments of Lake Cahuilla, The Borrego Mountain Earthquake of April 9, 1968, *U.S. Geol. Surv. Profess. Pap. 787*, 112–130.

Clark, M. M., K. K. Harms, J. J. Lienkaemper, D. S. Harwood, K. R. Lajoie, J. C. Matti, J. A. Perkins, M. J. Rymer, R. V. Sarna-Wojcicki, R. V. Sharp, J. D. Sims, J. C. Tinsley, and J. I. Ziony (1984). Preliminary slip-rate table for late Quaternary faults of California, *U.S. Geol. Surv. Open-File Rept. 84-106*, 12 pp.

Given, D., L. Hutton, and L. M. Jones (1987). *The Southern California Network Bulletin*, July–December 1986, *U.S. Geol. Surv. Open-File Rept. 87-488*, 28 pp.

Gutenberg, B. and C. F. Richter (1944). Frequency of earthquakes in California, *Bull. Seism. Soc. Am.* **34**, 185–188.

Hanks, T. and H. Kanamori (1979). A moment magnitude scale, *J. Geophys. Res.* **84**, 2348–2350.

Harden, J. W. and J. C. Matti (1989). Holocene and late Pleistocene slip rates on the San Andreas Fault in Yucaipa, California, using displaced alluvial-fan deposits and soil chronology, *Geol. Soc. Am. Bull.* **101**, 1107–1117.

Hauksson, E. and S. Gross (1991). Source parameters of the 1933 Long Beach earthquake, *Bull. Seism. Soc. Am.* **81**, 81–98.

Hudnut, K. W. and K. E. Sieh (1989). Behavior of the Superstition Hills fault during the past 330 years, *Bull. Seism. Soc. Am.* **79**, 304–329.

Ishimoto, M. and K. Iida (1939). Observations sur les seisms enregistre par le microseismograph construite dernierment (I), *Bull. Earthquake Res. Inst. Univ. Tokyo* **17**, 443–478.

Jacoby, G. C., P. R. Sheppard, and K. E. Sieh (1988). Irregular recurrence of large earthquakes along the San Andreas Fault: evidence from trees, *Science* **241**, 196–199.

Kagan, Y. (1993). Statistics of characteristic earthquakes, *Bull. Seism. Soc. Am.* **83**, 7–24.

Keller, E. A., M. S. Bonkowski, R. J. Korsch, and R. J. Shlemon (1982). Tectonic geomorphology of the San Andreas fault zone in the southern Indio Hills, Coachella Valley, California, *Geol. Soc. Am. Bull.* **93**, 45–56.

Klinger, R. E. and T. K. Rockwell (1989). Recurrent late Holocene faulting at Hog Lake in the Anza seismic gap, San Jacinto fault zone, southern California (abstracts with programs), *Geol. Soc. Am. 42*, 102.

Lindh, A. G. (1983). Preliminary assessment of long-term probabilities for large earthquakes along selected fault segments of the San Andreas fault system in California, *U.S. Geol. Surv. Open-File Rept. 83-63*, 1–15.

Lindvall, S. C., T. K. Rockwell, and K. W. Hudnut (1989). Slip distribution of prehistorical earthquakes on the Superstition Hills Fault, San Jacinto Fault zone, southern California, based on off-

set geomorphic features (abstracts with programs), *Geol. Soc. Am.* **21**, 107.

Magistrale, H., L. Jones, and H. Kanamori, (1989). The Superstition Hills, California, earthquakes of 24 November 1987, *Bull. Seism. Soc. Am.* **79**, 239–251.

McGill, S. and K. Sieh (1992a). Holocene slip rate of the central Garlock fault in southeastern Searles Valley, California, *J. Geophys. Res.* **98**, 14217–14231.

McGill, S. H. and K. E. Sieh (1991). Surficial offsets on the central and eastern Garlock fault associated with prehistoric earthquakes, *J. Geophys. Res.* **96**, 21597–21621.

Millman, D. E. and T. K. Rockwell (1986). Neotectonics of the Elsinore fault in Temescal Valley, California, in *Guidebook and Volume on Neotectonics and Faulting in Southern California*, Vol. 82, Geological Society of America, 159–166.

Pinault, C. T. and T. K. Rockwell (1984). Rates and sense of Holocene faulting on the southern Elsinore fault: further constraints on the distribution of dextral shear between the Pacific and North American plates (abstracts with programs), *Geol. Soc. Am.* **16**, 624.

Prentice, C. S., S. G. Wesnousky, and K. E. Sieh (1988). A minimum Holocene slip rate on the northern San Jacinto fault, San Bernardino Valley, southern California (abstracts with programs), *Geol. Soc. Am.* **20**, 222–223.

Richter, C. F. (1958). *Elementary Seismology*, W. H. Freeman, New York, 1–768.

Rockwell, T., C. Loughman, and P. Merifield (1990). Late Quaternary rate of slip along the San Jacinto fault zone near Anza, southern California, *J. Geophys. Res.* **95**, 8593–8605.

Rockwell, T. K., D. L. Lamar, R. S. McElwain, and D. E. Millman (1985). Late Holocene recurrent faulting on the Glen Ivy north strand of the Elsinore fault, southern California (abstracts with programs), *Geol. Soc. Am.* **17**, 404.

Rockwell, T. K., R. S. McElwain, D. E. Millman, and D. L. Lamar (1986). Recurrent Late Holocene faulting on the Glen Evy North Strand of the Elsinore fault at Glen Ivy Marsh, in *Guidebook and Volume on Neotectonics and Faulting in Southern California*, Vol. 82, Geological Society of America, 167–175.

Romanowicz, B. (1992). Strike-slip earthquakes on quasi-vertical transcurrent faults: inferences for general scaling relations, *Geophys. Res. Lett.* **19**, 481–484.

Salyards, S. L., Sieh, E. Kerry, and J. L. Kirschvink (1987). Paleomagnetic measurement of dextral warping during the past three large earthquakes at Pallett Creek, southern California (abstracts with programs), *Geol. Soc. Am.* **19**, 828.

Salyards, S. L., K. E. Sieh, and J. Kirshvinck (1992). Paleomagnetic measurement of non-brittle coseismic deformation across the San Andreas fault at Pallett Creek, *J. Geophys. Res.* **97**, 12457–12470.

Scholz, C. H. (1990). *The Mechanics of Earthquakes and Faulting*, Cambridge University Press, Cambridge, 439 pp.

Schwartz, D. P. and K. J. Coppersmith (1984). Fault behavior and characteristic earthquakes: examples from the Wasatch and San Andreas fault zones, *J. Geophys. Res.* **89**, 5681–5698.

Schwartz, D. P. and R. J. Weldon (1987). San Andreas slip rates; preliminary results from the 96 St. site near Littlerock, CA (abstracts with programs), *Geol. Soc. Am.* **19**, 448.

Sharp, R. V. (1981). Variable rates of late Quaternary strike slip on the San Jacinto fault zone, southern California, *J. Geophys. Res.* **86**, 1754–1762.

Sieh, K. (1986). Slip rate across the San Andreas Fault and prehistoric earthquakes at Indio, California, *EOS* **67**, 1200.

Sieh, K., M. Stuiver, and D. Brillinger (1989). A more precise chronology of earthquakes produced by the San Andreas Fault in Southern California, *J. Geophys. Res.* **94**, 603–623.

Sieh, K. E. (1978). Slip along the San Andreas Fault associated with the great 1857 earthquake, *Bull. Seism. Soc. Am.* **68**, 1421–1448.

Sieh, K. E. (1984). Lateral offsets and revised dates of large prehistoric earthquakes at Pallett Creek, southern California, *J. Geophys. Res.* **89**, 7641–7670.

Sieh, K. E. and R. H. Jahns (1984). Holocene activity of the San Andreas at Wallace Creek, California, *Geol. Soc. Am. Bull.* **95**, 883–896.

Sieh, K. E. and P. L. Williams (1990). Behavior of the southernmost San Andreas Fault during the past 300 years, *J. Geophys. Res.* **95**, 6629–6645.

Sykes, L. R. and S. P. Nishenko (1984). Probabilities of occurrence of large plate rupturing earthquakes for the San Andreas, San Jacinto, and Imperial faults, California, 1983–2003. *J. Geophys. Res.* **89**, 5905–5927.

Toppozada, T. R. and D. L. Parke (1982). Areas damaged by California earthquakes, 1900–1949, *Calif. Div. Mines Geol. Open-File Rept. 82-17*, 65 pp.

Vaughan, P. and T. K. Rockwell (1986). Alluvial stratigraphy and neotectonics of the Elsinore Fault Zone at Agua Tibia Mountain, southern California, in *Guidebook and Volume, 82nd Annual Meeting of the Cordilleran Section of the Geological Society of America*, Vol. 82, 177–191.

Weldon, R. J. (1991). Active tectonic studies in the United States, 1987–1990, Reviews of Geophysics Supplement, U.S. National Report to International Union of Geodesy and Geophysics 1987–1990, American Geophysical Union, Washington, D.C., 890–906.

Weldon, R. J. and K. E. Sieh (1985). Holocene rate of slip and tentative recurrence interval for large earthquakes on the San Andreas Fault, Cajon Pass, southern California, *Geol. Soc. Am. Bull.* **96**, 793–812.

Wesnousky, S. G. (1986). Earthquakes, Quaternary faults, and seismic hazard in California, *J. Geophys. Res.* **91**, 12587–12631.

Wesnousky, S. G. (1988). Seismological and structural evolution of strike-slip faults, *Nature* **335**, 340–343.

Wesnousky, S. G. (1990). Seismicity as a function of cumulative geologic offset: some observations from southern California, *Bull. Seism. Soc. Am.* **80**, 1374–1381.

Wesnousky, S. G., C. H. Scholz, K. Shimazaki, and T. Matsuda (1983). Earthquake frequency distribution and the mechanics of faulting, *J. Geophys. Res.* **88**, 9331–9340.

Working Group on California Earthquake Probabilities (1988). Probabilities of large earthquakes occurring in California on the San Andreas Fault, *U.S. Geol. Surv. Open-File Rept. 83-398*, 35 pp.

Working Group on California Earthquake Probabilities (1990). Probabilities of large earthquakes in the San Francisco Bay region, California, *U.S. Geol. Surv. Circular 1053*, 51.

Youngs, R. and K. Coppersmith (1985). Implications of fault slip rates and earthquake recurrence models to probabilistic hazard estimates, *Bull. Seism. Soc. Am.* **75**, 939–964.

Center for Neotectonic Studies
and Department of Geological Sciences
University of Nevada–Reno
Reno, Nevada 89557

Manuscript received 5 April 1993.